Green Chemistry

Accepted Manuscript

ROYAL SOCIETY OF CHEMISTRY

www.rsc.org/greenchem

Cite this: DOI: 10.1039/c0xx00000x

www.rsc.org/xxxxxx

ARTICLE TYPE

Highly efficient and reversible CO_2 adsorption by amine-grafted platelet SBA-15 with expanded pore diameter and short mesochannels

Lingyun Zhou,[a,b] Jing Fan, *[a] Guokai Cui,[a] Xiaomin Shang,[a] Qinghu Tang,[a] Jianji Wang*[a] and Maohong Fan[c]

Received (in XXX, XXX) Xth XXXXXXXXX 200X, Accepted Xth XXXXXXXXX 200X
DOI: 10.1039/b000000x

The ever-increasing concentration of CO_2 in the atmosphere has raised great concerns over carbon capture techniques. To enhance CO_2 adsorption capacity, a kind of platelet SBA-15 with short channels and large pore diameter has been prepared and grafted with various aminosilanes (mono-, di-, and tri-amine). Thorough analysis of the support structure and sorbent performance was estimated through a combination of amine loading, CO_2 adsorption capacity and CO_2/N_2 selectivity. It was shown that compared to traditional fiber SBA-15, amine loading for these novel sorbents was increased from 3.56 to 5.90 mmol/g (a 66% increase), and the CO_2 adsorption capacity was increased from 1.23 to 2.67 mmol/g (a 120% increase). Also, the selectivity of CO_2/N_2 was remarkably enhanced from 37 to 169. The CO_2 adsorption enthalpy reached 67 kJ mol^{-1}. Moreover, these sorbents are regenerable and exhibit good stabilities. Thus, this approach offers an alternative for the development of technological innovation towards efficient and reversible processes for carbon capture.

Introduction

Due to increasing emission amounts of CO_2 from fossil fuel combustion and enhancement of the greenhouse effect, the carbon capture and storage (CCS) have attracted increasing attention. As an extensively applied technique, amine-based aqueous processes have several drawbacks such as relatively low CO_2 adsorption capacity, potential toxic byproduct release, operational instability and frequent equipment maintenance due to excessive corrosion of the amine system, and high energy consumption. Consequently, a number of alternative capture techniques have been developed in the past years,[1-4] such as membrane separation[5-7], ionic liquid absorption[8, 9] and solid adsorption technologies[10, 11]. Among the various CCS technologies, gas phase adsorption technologies on porous adsorbents such as silica materials,[12] carbon materials[13] and Metal–Organic Frameworks (MOFs)[14] have been the focus of many investigations due to their economical, noncorrosive and eco-friendly advantages.[15, 16]

Two different pathways have been explored for searching efficient sorbents: enhancing the physical adsorption capacities by increasing the surface area of the sorbents and improving the chemical adsorption capacities by chemically modification.[17, 18] Among these porous sorbents, amine-functionalized mesoporous silica materials attracted considerable attention as a promising chemical sorbent due to their tunable structures and controllable surface chemistry. In addition, CO_2 binds to amine group to form carbamate or carbamic acid,[19] resulting in selective adsorption of CO_2.[20]

According to their preparation methods, amine-functionalized mesoporous silica materials can be classified into (I) physical impregnation of mesoporous materials with amine-rich polymers[21, 22] and (II) chemical reaction of organic amines with nanoporous inorganic materials.[23, 24] Although class I adsorbents usually have significantly enhanced amine loading, amine leaching could occur usually because of the weak interaction between amine group and the supports. By contrast, amine groups of class II adsorbents are covalently bonded to the supports, thus these amine-functionalized materials have high thermal stability. In addition, higher porosity allows for faster kinetics.[25]

In recent years, a series of amine-grafted sorbents have been developed based on mesoporous silica materials such as SBA-15, SBA-16 and MCM-41. Although they show fast CO_2 adsorption kinetics and enhanced capacities compared to those based on aqueous amine solutions, some of the disadvantages of this type of sorbents, including pore (Knudsen) diffusion and accessibility limitations, still need to be overcome.[26] Thus the performance of sorbents needs to be further improved. Recently, it has been demonstrated that particle morphology and pore size of mesoporous silica supports have significant effects on their CO_2 capture performances. For example, the pore-expansion of mesostructured materials can offer some advantages such as incorporating a higher amino content and simultaneously avoiding diffusion restrictions[27]. The use of pore-expanded solid supports such as PE-SBA-15[27-29] and PE-MCM-41[30, 31] exhibited higher adsorption efficiencies of the amino groups and better CO_2

[a] *School of Chemistry and Environmental Science, Henan Normal University, Xinxiang, 453007, China; Fax: +86-373-3329030; E-mail: fanjing@henannu.edu.cn (J. Fan); Jwang@henannu.edu.cn (J. Wang)*
[b] *College of Resource and Environment, Henan Institute of Science and Technology, Xinxiang, Henan 453007 (P.R. China)*
[c] *Department of Chemical and Petroleum Engineering, University of Wyoming, Laramie, Wyoming 72071(United States)*
† Electronic Supplementary Information (ESI) available: Experimental procedure and Table S1, Table S2, Table S3, Fig. S1, Fig. S2, Fig. S3. See DOI: 10.1039/b000000x/

capture than their conventional counterparts when functionalizing them either by grafting or impregnation on the different supports. Apart from the pore size, the pore length of the silica supports is also an important factor affecting CO_2 capture capacity due to molecular diffusion through the lengthy mesochannels and pore blockage along the channels. The mesoporous silica materials with short mesochannels have been found favorable in catalysis[32, 33] and enzymeimmobilization,[34, 35] which were synthesized by adding co-surfactant, co-solvent,[36] electrolyte[37] or organosilane[38] into the solutions. Heydari-Gorji *et al.*[39] reported that adsorbents with a shorter pore length outperformed materials with longer channels in terms of CO_2 uptake. Nevertheless, this effect on the CO_2 adsorption capacities was limited to amine impregnated materials, but not for amine-grafted mesoporous silica materials. The improvement of CO_2 mass transfer by both shortening mesochannels and expanding pore diameter inspires us to develop a new method for efficient and reversible CO_2 adsorption with the purpose of capacity-increasing and energy-saving.

In this work, we have prepared the platelet mesoporous silica support materials with short channels and expanded pores (hereinafter referred as SBA-15-p) using zirconyl chloride octahydrate ($ZrOCl_2$•$8H_2O$), pluronic 123 (P123, Mw = 5800) and 1,3,5-trimethylbenzene (TMB) according to the procedure reported in literature,[40] and then grafted them with three kinds of aminosilanes, 3-amino propyltrimethoxysilane (APTMS), N-(3-(trimethoxysilyl)propyl)ethane-1,2-amine (APAETMS) and 3-[2-(2-aminoethylamino)ethylamino] propyltrimethoxysilane (APAEAETMS), for preparations of three types of silica materials with mono-, di- or tri-amine sites per molecule grafted to the silica surface (see Scheme 1 for their structures). Moreover, the important performances, such as selectivity, regeneration and stability of these amine-functionalized mesoporous silica materials were extensively investigated. It was confirmed that this platelet morphology could offer the sorbent support a greater loading of amine and show better performance for CO_2 adsorption through short channels and large pore diameters. Additionally, these sorbents showed high CO_2/N_2 selectivity and good regeneration performance. For comparison, traditional fiber like SBA-15 (hereinafter referred as SBA-15-f) and its derived sorbents were also synthesized, as reported elsewhere.[41]

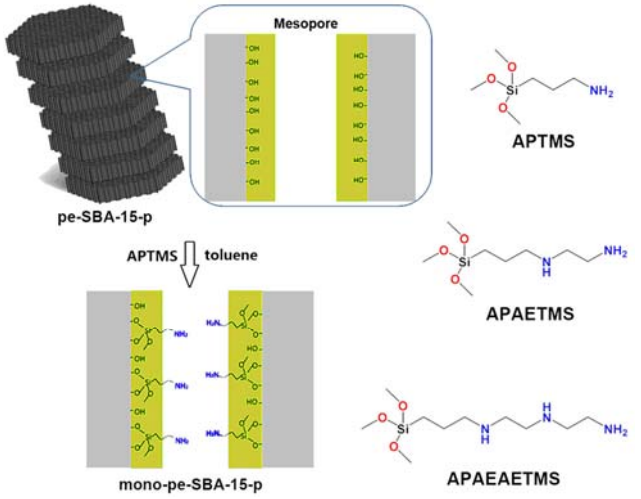

Scheme 1. Synthetic route of mono-SBA-15-p from SBA-15-p and APTMS, and the structures of APTMS, APAETMS and APAEAETMS.

Results and Discussion

Structure and morphology of the sorbents

The SEM images of SBA-15-p and SBA-15-f are shown in Figure 1. Significant differences in the morphologies of SBA-15-p and SBA-15-f samples can be clearly observed. With the Zr incorporation, clear platelet morphology of SBA-15-p (Fig. 1a) appeared in comparison with the original fiber-like structure of SBA-15-f (Fig. 1c), and Zr intense pocket was observed in the SEM–EDS analysis, as shown in Figure 1d. Hexagonal prism-like morphology of SBA-15-p was presented with a mesochannels length of *ca.* 200 nm and a particle size of 1-2 μm (Fig. 1b). The structure of SBA-15-p by high-SEM was also investigated (Fig. S1), in which the mesochannels structure can be observed but not clearly, and the image magnified scale is close to that in the TEM. Meanwhile, it was found from TEM images (Fig. 2) that the synthesized SBA-15-p material had an ordered hexagonal structure, while the pore diameter was enlarged by swelling the P123 micelles with TMB molecules and the pore structure did not collapse.

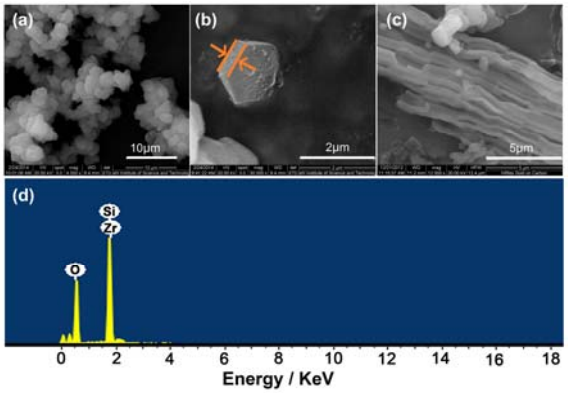

Fig. 1 Upper: SEM images of (a) piled morphologies of SBA-15-p, (b) single particle of SBA-15-p and (c) SBA-15-f; lower: (d) EDS analysis of SBA-15-p.

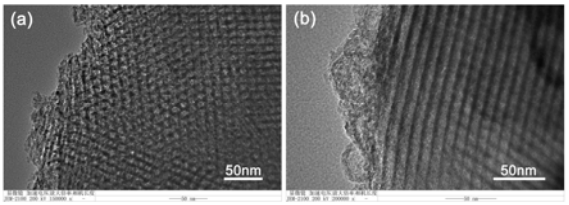

Fig. 2 (a) TEM image of SBA-15-p and (b) TEM image obtained after the specimen was tilted by more than 30°.

The structures of SBA-15-p, SBA-15-f and their derived sorbents were also investigated with X-ray diffraction (XRD) and nitrogen physic-sorption. The small-angle XRD patterns of sorbent supports were shown in Fig. 3a. It was found that the SBA-15-p and SBA-15-f contained the characteristic peaks of the (100), (110) and (200) planes. The retention of three characteristic peaks after TMB swelling and Zr modification confirms that SBA-15-p has the same 2D hexagonal p6mm pore structure as the traditional SBA-15-f, which is consistent with the morphology observed in the TEM images. Furthermore, the intensity of the peaks had not changed considerably compared to those of SBA-15-f, indicating the good order of the pore structure

since the diffraction peak intensity is correlated with the scattering contrast between the silicate walls and the pores. However, the diffraction peaks of SBA-15-p shift slightly toward lower angles than SBA-15-f, which would be attributed to the increase in pore diameter.[42]

Basically, similar XRD patterns as sorbent supports were found for the derived sorbents, mono-SBA-15-p and mono-SBA-15-f samples (Fig. 3b). It can be seen that diffraction intensity of (110) plane became weaker, thus indicating the less ordering of the pore structure for these sorbents due to the filling of amine in the mesopores.

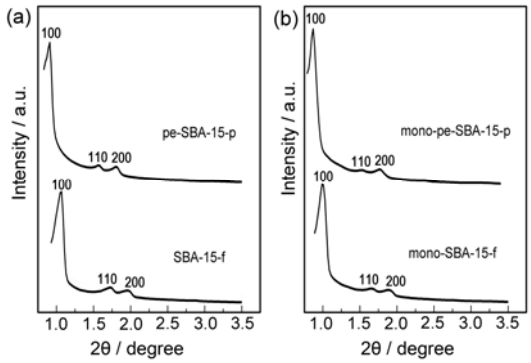

Fig. 3 XRD patterns of (a) SBA-15-p and SBA-15-f, (b) mono-SBA-15-p and mono-SBA-15-f.

For both sorbent supports, N_2 adsorption-desorption isotherms at -196 °C exhibited characteristic features of the type IV isotherm with its parallel H1 type hysteresis loop, indicating the presence of well-ordered mesopores (Fig. 4a). The hysteresis loops of SBA-15-p shifted toward lower P/P_0 regions compared to SBA-15-f. After immobilization of APTMS, N_2 adsorption on mono-SBA-15-p and mono-SBA-15-f were clearly reduced when compared to SBA-15-p and SBA-15-f (Fig. 4b). The reductions resulted from the pore clogging and increased weight from the grafted amine group.

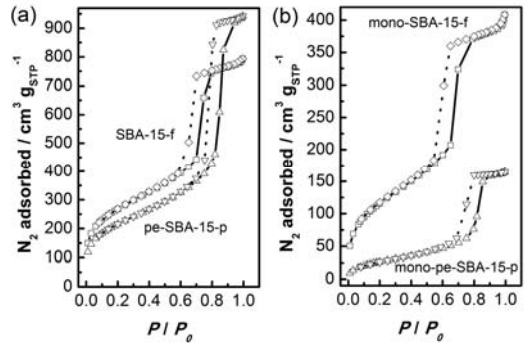

Fig. 4 N_2 isotherms at -196 °C of (a) SBA-15-p and SBA-15-f, (b) mono-SBA-15-p and mono-SBA-15-f (sorption: solid line; desorption: dot line).

The Brunauer-Emmett-Teller (BET) surface area, pore volumes and pore diameters of all samples were summarized in Table 1. On the whole, with increase in the number of amine groups in grafted-aminosilane, BET surface areas, pore volumes and pore diameters of the sorbents with the same support decreased regardless of SBA-15-p or SBA-15-f, mainly because more amine groups were grafted on the support. The pore size distribution center of the Barrett-Joyner-Halenda (BJH) was at 14.7 nm for SBA-15-p and 7.5 nm for SBA-15-f, respectively (Table 1). Due to the large pore size, the BET surface area of SBA-15-p (752 m^2 g^{-1}) was a little lower than that of SBA-15-f (906 m^2 g^{-1}). At the same time, the pore volume increased from 1.23 to 1.46 cm^3 g^{-1} (Table 1). Also, the BET surface area was reduced dramatically from 752 m^2 g^{-1} for SBA-15-p to 100 m^2 g^{-1} for mono-SBA-15-p, as compared with the decrease from 906 m^2 g^{-1} for SBA-15-f to 406 m^2 g^{-1} for mono-SBA-15-f. This suggests that more amine groups were immobilized onto mono-SBA-15-p.

Table 1. Textural characteristics of the supports before and after amine immobilization.

Sample	Surface area, SBET[a] /m^2 g^{-1}	Pore volume, Vtotal[b] /cm^3 g^{-1}	Pore diameter, dp[c] /nm
SBA-15-p	752	1.46	14.7
mono-SBA-15-p	100	0.25	12.2
di-SBA-15-p	88	0.22	12.0
tri-SBA-15-p	47	0.18	11.7
SBA-15-f	906	1.23	7.5
mono-SBA-15-f	406	0.63	6.2
di-SBA-15-f	373	0.60	6.1
tri-SBA-15-f	318	0.54	6.0

[a] Surface area was calculated using the BET method at P/P_0=0.05-0.2; [b] values at P/P_0=0.99; [c] most probable pore size estimated by the BJH method from the isotherm of adsorption branch.

Effect of the grafted amine loadings on CO_2 adsorption capacity

The calculated amine loading amounts of the sorbents were shown in Table 2. For the same sorbent supports, it was found that the increase of the amine group number results in a higher amine loading on the sorbents. For example, the loaded amounts of nitrogen on mono-SBA-15-p, di-SBA-15-p and tri-SBA-15-p were 2.37, 3.88 and 5.90 mmol N g^{-1} adsorbent, respectively. This is because the -OH densities used for grafting for the same sorbent supports are identical, and the loading amounts of nitrogen are directly related to the number of amine groups of precursors in the absence of sterically inaccessibility. Even more, it was observed that the platelet morphology with short channels and large pore diameters offers SBA-15-p more amine loading than SBA-15-f for the same amine precursor, such as 2.37 mmol N g^{-1} adsorbent for mono-SBA-15-p versus 1.48 mmol N g^{-1} for mono-SBA-15-f. This can be ascribed to more efficient diffusion and higher sterically accessibility resulting from short channels and large pore sizes.

Table 2 also compared CO_2 adsorption performance by these sorbents with different morphologies and different number of amine groups. It was shown that SBA-15-p derived sorbents exhibited greater adsorption capacity than that derived from SBA-15-f. For example, the capacity of CO_2 adsorption was increased from 0.99 mmol g^{-1} by mono-SBA-15-f to 1.58 mmol g^{-1} by mono-SBA-15-p. We also calculated CO_2 adsorption capacities using the data of BET surface area, and found that the CO_2 adsorption capacity of mono-SBA-15-p was 1.58×10^{-2} mmol m^{-2}, which is 6.6 times that of mono-SBA-15-f (0.24×10^{-2} mmol m^{-2}).

Table 2. Comparisons of the aminosilanes immobilized SBA-15-p and SBA-15-f as adsorbents.

Sample	loaded of N /mmol g^{-1}	CO_2 adsorption /mmol g^{-1}(mmol m^{-2})	C/N[a] /mol mol^{-1}
mono-SBA-15-p	2.37	1.58 (1.58×10^{-2})	0.67
di-SBA-15-p	3.88	2.01 (2.28×10^{-2})	0.52
tri-SBA-15-p	5.90	2.67 (5.69×10^{-2})	0.45
mono-SBA-15-f	1.48	0.99 (0.24×10^{-2})	0.67
di-SBA-15-f	2.27	1.15 (0.31×10^{-2})	0.50
tri-SBA-15-f	3.56	1.23 (0.39×10^{-2})	0.34

[a] C/N = mole number of the captured CO_2 per mole of grafted amine group in 1.0 g of adsorbent.

Another important feature of these sorbents on CO_2 adsorption performance is that the increase of amine loading amounts results in the enhanced CO_2 adsorption capacity. For example, the capacities of CO_2 adsorption were increased from 1.58 mmol g^{-1} by mono-SBA-15-p to 2.67 mmol g^{-1} by tri-SBA-15-p and from 0.99 mmol g^{-1} by mono-SBA-15-f to 1.63 mmol g^{-1} by tri- SBA-15-f, respectively. To our surprise, through changing precursor from APTMS to AEAEAPTMS, 68% increase of CO_2 capacity by SBA-15-p derived sorbents was observed, which was about two times higher than that (23%) by the SBA-15-f derived sorbents. This indicates that CO_2 adsorptions by former are more accessible and efficient through decreasing transport limitations.

In addition, we defined the mole of captured CO_2 per mole of grafted amine group as C/N (Table 2) in order to study amine efficiency on CO_2 adsorption. However, it is worthy to mention that C/N is not quite the same as amine efficiency, because the contribution to CO_2 capacities by amine-grafted sorbents is determined not only by chemisorption of amine group but also by physisorption of surface area. Since the amine-grafted SBA-15-f derived sorbents have larger surface areas, it is clearly indicated that the amine-grafted SBA-15-p derived sorbents possess higher amine efficiency.

CO_2 isotherms

The CO_2 adsorption-desorption isotherms of mono-SBA-15-p and mono-SBA-15-f were determined at 25 °C (Fig. 5). A large increase at pressure <0.1 bar was observed for both sorbents. The adsorption of CO_2 at pressure <0.1 bar was attributed to the chemical reaction between CO_2 and the grafted amine group, while the linearity of the isotherms was suggested to be physisorption between 0.1 and 1.0 bar. It is clear that CO_2 adsorption capacity by mono-SBA-15-f was largely attributed to physisorption due to its larger BET surface area.

In addition, it was found that although the amine loading amount presented by mono-SBA-15-p was approximately 1.6 times that by mono-SBA-15-f, CO_2 adsorption capacity of the former (*ca.* 1.30 mmol g^{-1}) was about 2.4 times that of the latter (*ca.* 0.55 mmol g^{-1}) at 0.1 bar of the isotherms. It is assumed that the grafted amines have been consumed at <0.1 bar, and the theoretical value for the amine efficiency is 0.5, where two amines could capture one CO_2[43]. For mono-SBA-15-p, the amine efficiency (the mole of captured CO_2 per mole of grafted amine group at 0.1 bar) was 0.51, very close to the theoretical value. The platelet structure in short channels and large pores generated more efficient CO_2 diffusion and provided enough space in the inner layer to avoid the steric hindrance effect. Thus most of the adsorption sites on mono-SBA-15-p are highly accessible. By contrast, the amine efficiency of mono-SBA-15-f was only 0.27, much lower than the theoretical value. It is speculated that some amines grafted in the inner layer of the materials could be isolated from other amines due to the tubular structure and other steric effects, and these amines can not be reached for the CO_2 adsorption.

It can also be seen from Fig. 5 that there was obviously hysteresis between the CO_2 adsorption and desorption branches on mono-SBA-15-p. The hysteresis phenomena would be caused by the incomplete desorption of CO_2 at 25 °C. Thus the interaction between CO_2 and amine groups is so strong that more energy is required to break it.[44, 45]

A comparison was made for our amine-grafted SBA-15-p with other related materials reported in the literatures (Table S3). It was found that both CO_2 adsorption capacity and amine efficiency of the amine-grafted SBA-15-p were comparable with those of amine-derived ionic liquids.[8, 9] Compared with porous solid materials immobilized with amine-rich precursors,[10, 11] amine-grafted SBA-15-p exhibited lower CO_2 adsorption capacity but higher amine efficiency. Because only a monolayer of sites was formed on typical mesoporous silica supports, amine-grafted SBA-15-p tended to have more open porosity, resulting in fewer diffusion limitations and potentially faster adsorption and desorption kinetics.

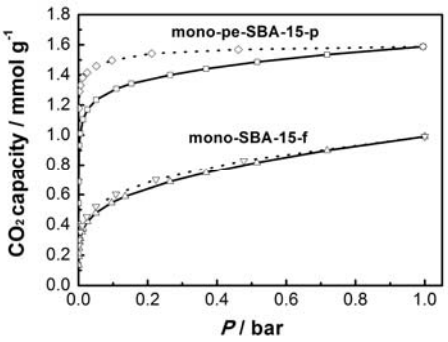

Fig. 5 CO_2 isotherms on mono-SBA-15-p and mono-SBA-15-f at 25 °C (sorption: solid line; desorption: dot line).

Effect of temperature on the CO_2 adsorption performance

To study the effect of temperature on the CO_2 adsorption performance, the CO_2 adsorption isotherms at 25, 35 and 50 °C on mono-SBA-15-p were measured (Fig. 6). It could be seen that CO_2 adsorption capacity decreased with the increase of adsorption temperature. For example, CO_2 adsorption capacities at 25, 35, 50 °C and 1 bar were 1.59, 1.46 and 1.35 mmol g^{-1}, respectively. However, they were very close to each other at relatively low pressure. Their obvious difference at high pressure results from stronger physisorption, while they exhibit a close chemical adsorption capacity at 0.1 bar because of the reaction of CO_2 with the immobilized amine. Meanwhile, dry and wet CO_2 uptakes on the mono-SBA-15-p were measured by breakthrough curves to investigate the influence of moisture on CO_2 adsorption (Fig. S2). It was shown that more CO_2 was adsorbed under wet conditions. That is, a positive effect was found for CO_2 capture in the presence of water vapor.

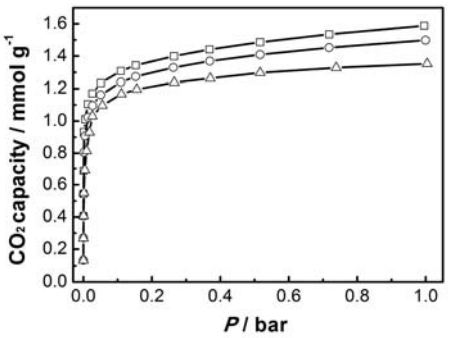

Fig. 6 CO_2 adsorption isotherms on mono-SBA-15-p at 25 °C (□), 35 °C (○) and 50 °C (△).

The enthalpy of the CO_2 adsorption

The isosteric heats of adsorption ΔH_q on mono-SBA-15-p were calculated from the CO_2 isotherms at 25, 35 and 50 °C by Clausius−Clapeyron equation

$$\ln P_q = \frac{\Delta H_q}{RT} + C \qquad (1)$$

in which P_q represents the pressure at a fixed adsorbed amount q and C is a constant. The isosteric heats of adsorption have been calculated from the slope of the linear plot of ln$P$ against 1/T at the same adsorbed quantity.

The fitting plots by Clausius−Clapeyron equation at three different adsorption amounts were depicted in Fig. 7 and good straight lines were found. It is clearly indicated that the isosteric heats of adsorption on mono-SBA-15-p declined from 67.1 kJ mol^{-1} (at q = 0.55 mmol g^{-1}) to 50.3 kJ mol^{-1} (at q = 1.0 mmol g^{-1}) and 49.6 kJ/mol (at q = 1.3 mmol g^{-1}). The corresponding adsorption heats for other amine-modified mesoporous silicas were reported to be in the range of 45-95 kJ mol^{-1},[23, 46-48] while those for pure mesoporous silicas, zeolites and metal-organic frameworks mainly based on the physisorption were 30-50 kJ mol^{-1}.[23, 49, 50] Compared to these values, it is clear that the major mechanism of CO_2 adsorption on the mono-SBA-15-p was not the physisorption by the silica surface but the chemisorption by the amine groups.

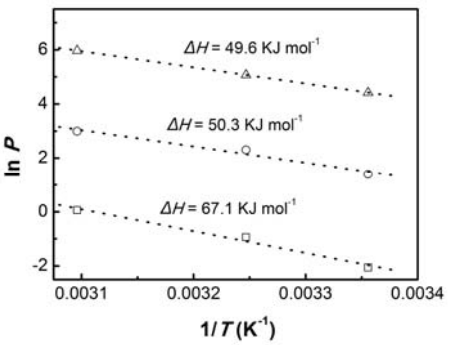

Fig. 7 Variation of lnp with 1/T at q = 0.55 mmol g^{-1}(□), 1.00 mmol g^{-1}(○), and 1.30 mmol g^{-1}(△) of mono-SBA-15-p. The dot lines are the fits of Clausius−Clapeyron equation at different q values.

Generally, owing to the surface heterogeneity, the value of the adsorption heat decreases with the increase in the quantity of the adsorbate adsorbed. That is to say, the higher the activities of the sorption sites, the larger the value of adsorption heat. Within low adsorption capacity range, (e. g. 0.55 kJ mol^{-1}), CO_2 can be adsorbed relatively easily. With the increase in CO_2 adsorption, the availability of sorption sites decreases. Actually, CO_2 molecules need to transfer to relatively inaccessible sites in the interior pores of sorbents, which leads to the decrease in the adsorption heat.

Effects of adsorption times on the extent of adsorption

The effect of adsorption times on the extent of adsorption is very important to show the different adsorption performances by mono-SBA-15-p and its fiber-structure counterpart. Thus, we have examined the effect of adsorption times on the extent of adsorption, for a few selected points (pressure values), on the isotherms of platelet and fiber-like samples. The Isotherm Tabular Reports of raw data in the Analyzer for mono-SBA-15-p and mono-SBA-15-f were shown in Table S1 and Table S2, respectively. It can be seen that under the approximately equal pressure, the equilibrium of CO_2 on the mono-SBA-15-p adsorbents needs longer time than that on the mono-SBA-15-f. For example, the equilibrium adsorption times of CO_2 on mono-SBA-15-p and mono-SBA-15-f adsorbents under about 19.8 mmHg are 60 h 51 min and 17 h 42 min, respectively. This means lower saturation of CO_2 molecules in the fiber sample compared to the platelet sample, and better adsorption performance of mono-SBA-15-p over its fiber-structure counterpart.

CO_2/N_2 selectivity

To investigate the selectivity of CO_2/N_2, we compared N_2 adsorption isotherms at 25 °C on mono-SBA-15-p and mono-SBA-15-f with the corresponding CO_2 adsorption isotherms (Fig. 8). It was seen that the N_2 adsorption capacities at 25 °C and 1 bar on mono-SBA-15-p and mono-SBA-15-f were 0.0094 mmol g^{-1} and 0.027 mmol g^{-1}, respectively, thus CO_2/N_2 selectivity by mono-SBA-15-p (169) was remarkably higher than that by mono-SBA-15-f (37). Considering the fact that the flue gases from power plants consist of ~70% N_2 and ~15% CO_2 at the pressure of ~1 bar,[51] a comparison was also made for the CO_2/N_2 sorption selectivity of the two absorbents by calculating CO_2 adsorption capacities at 0.15 bar and N_2 adsorption capacities at 0.70 bar. It was found that CO_2/N_2 sorption selectivity increased from 30 for mono-SBA-15-f to 195 for mono-SBA-15-p. These results indicated that the platelet morphology with large pore diameters could greatly enhance CO_2/N_2 sorption selectivity. While the platelet morphology with large pore diameters offered SBA-15-p more amine loading, BET surface area was dramatically reduced from 752 m^2 g^{-1} for SBA-15-p to 100 m^2 g^{-1} for mono-SBA-15-p. This greatly reduced the physical adsorption of N_2 molecules. On the other hand, there is no chemical absorption between amine group and N_2 molecules. The combination of both results in the high CO_2/N_2 selectivity of mono-SBA-15-p, particularly at low CO_2 partial pressures.

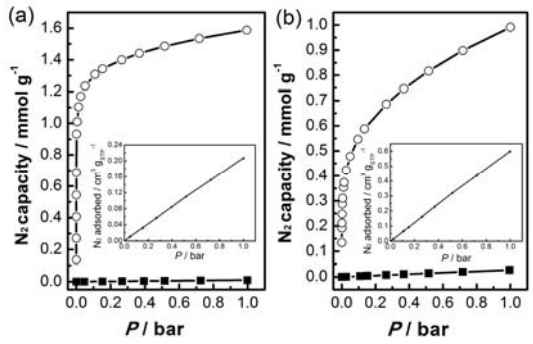

Fig. 8 CO_2 (○) and N_2 (■) isotherms on (a) mono-SBA-15-p and (b) mono-SBA-15-f at 25 °C.

Regeneration and stability of the adsorbents

Stability of the sorbents would be the determinant for the application of the adsorbents in practical CO_2 capture. In order to evaluate the stability of our sorbents, cyclic CO_2 adsorption-desorptions on mono-SBA-15-p were performed. After each adsorption, mono-SBA-15-p was regenerated under vaccum of 10^{-8} bar for 8 h at 90 °C. After ten cycles of adsorption-desorption, CO_2 adsorption isotherms on mono-SBA-15-p was measured at 25 °C and compared to that with the first adsorption isotherm (Fig. 9a). It could be seen that the adsorption isotherms on mono-SBA-15-p and CO_2 sorption capacities showed virtually no change after 10 adsorption-desorption cycles (Fig. 9b). This indicates that the mono-SBA-15-p sorbent is stable.

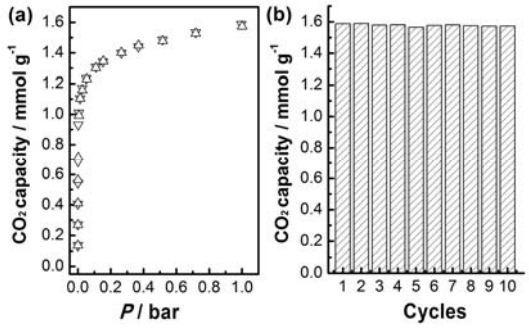

Fig. 9 (a) CO_2 adsorption isotherms on mono-SBA-15-p for the first adsorption (△) and the tenth adsorption (▽) at 25 °C; (b) Ten CO_2 adsorption-desorption cycles on mono-SBA-15-p at 25 °C.

Solid NMR, IR and TGA investigations

To study the adsorption mechanism of the adsorbents for CO_2 in depth, we performed attenuated total reflectance infrared (ATR-IR) absorption measurements of the absorbent before and after CO_2 uptake (Fig. 10). It is shown that after CO_2 absorption, the peak of the neat absorbent at around 1594 cm^{-1}, assigned to the -NH_2 bending mode of the primary amine,[52] disappeared completely. At the same time, an intense absorption at 1490 cm^{-1} is observed, which is assigned to the NH_3^+ absorption.[53, 54] Also we observe a band at ~1564 cm^{-1} that is consistent with the expected position of the asymmetric stretching mode of COO^-.[55, 56] These observations suggest the formation of alkylammonium carbamate stabilized by the nearest neighbor amine interactions. It is postulated that the formation of the NH_3^+ carbamate counterion involves the transfer of a proton from the primary amine forming the carbamate to a nearest neighbor amine.

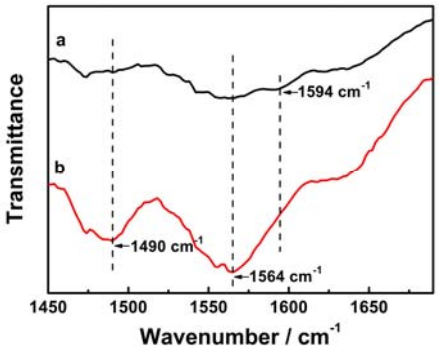

Fig. 10 ATR-IR spectra formono-SBA-15-p after CO_2 uptake (a) and fresh mono-SBA-15-p samples (b).

To identify this mechanism, ^{13}C CP MAS NMR spectra of mono-SBA-15-p before and after CO_2 uptake were determined and shown in Fig. 11. In addition to the signals below 60 ppm associated with the propyl carbon chain, the mono-SBA-15-p sample exhibited an obvious signal at 163.8 ppm after CO_2 uptake, which was attributed to carbamate. Meanwhile, the frech sample presented a weak peak at 163.8 ppm due to the adsorption of atmospheric CO_2.[8, 57] TGA thermograms of mono-SBA-15-p before and after CO_2 uptake in an air atmosphere were presented in Fig. S3. As it was shown, mono-SBA-15-p showed a total of 25.7% weight loss after CO_2 uptake, while for the fresh mono-SBA-15-p, the total weight loss was 21.3%. For both samples, the weight loss difference was more significant in the temperature range from 30 to 100 °C, which was attributed to the degradation of the chemisorbed CO_2.

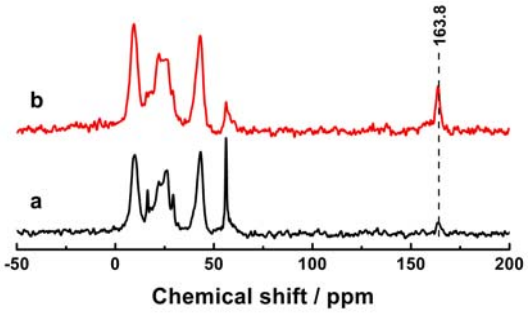

Fig. 11 ^{13}C CP MAS NMR spectra of mono-SBA-15-p: (a) before CO_2 uptake, (b) after CO_2 uptake.

Based on the previous reports and the above discussion, the mechanism of CO_2 absorption by mono-SBA-15-p is suggested and shown in Scheme 2. Thus the large CO_2 capture capacity of mono-SBA-15-p is mainly contributed from chemical absorption via the reaction between -NH_2 group and CO_2 molecules.

$$2R\text{-}NH_2 + CO_2 \rightarrow R\text{-}NHCOO^- + R\text{-}NH_3^+$$

Scheme 2. The reaction mechanism of CO_2 with amine (primary amine) groups on the absorbents.

Conclusions

In summary, highly efficient and reversible CO_2 adsorption by an amine-grafted sorbent based on platelet silica support with short channel and large pore diameter has been found. Compared with

conventional SBA-15-f derived sorbents, the SBA-15-p derived sorbents were more capable in CO_2 adsorption. The platelet morphology greatly enhanced CO_2 adsorption capacity since it can increase amine loading and improve amine efficiency, and directly increase CO_2/N_2 sorption selectivity. The adsorption heat associated with the CO_2 sorption on mono-aminosilanes grafted sorbent suggests that chemisorption dominated. Furthermore, the captured CO_2 can be released by heating under vacuum, and the adsorbent is quite stable after 10 adsorption-desorption cycles. The high adsorption capacity, CO_2/N_2 sorption selectivity and good stability could make this adsorbent promising for industrial application.

Acknowledgements

This work was supported by the National Natural Science Foundation of China (Grant No. 21377036) and the Innovation Scientists Projects of Henan Province (No. 092101510300).

Notes and references

1. D. M. D'Alessandro, B. Smit and J. R. Long, *Angew. Chem. Int. Ed.*, 2010, **49**, 6058-6082.
2. S. Cui, W. Cheng, X. Shen, M. Fan, A. Russell, Z. Wu and X. Yi, *Energy Environ. Sci.*, 2011, **4**, 2070-2074.
3. B. Dutcher, M. Fan, B. Leonard, M. D. Dyar, J. Tang, E. A. Speicher, P. Liu and Y. Zhang, *J. Phys. Chem. C*, 2011, **115**, 15532-15544.
4. L. He, M. Fan, B. Dutcher, S. Cui, X.-d. Shen, Y. Kong, A. G. Russell and P. McCurdy, *Chem. Eng. J.*, 2012, **189**, 13-23.
5. Q. Jiang, S. Faraji, K. J. Nordheden and S. M. Stagg-Williams, *J. Membr. Sci.*, 2011, **368**, 69-77.
6. P. Li, D. R. Paul and T. S. Chung, *Green Chem.*, 2012, **14**, 1052-1063.
7. L. Xiong, S. Gu, K. O. Jensen and Y. S. Yan, *ChemSusChem*, 2014, **7**, 114-116.
8. C. Wang, Y. Guo, X. Zhu, G. Cui, H. Li and S. Dai, *Chem. Commun.*, 2012, **48**, 6526-6528.
9. X. Y. Luo, F. Ding, W. J. Lin, Y. Q. Qi, H. R. Li and C. M. Wang, *J. Phys. Chem. Lett.*, 2014, **5**, 381-386.
10. J. C. Hicks, J. H. Drese, D. J. Fauth, M. L. Gray, G. Qi and C. W. Jones, *J. Am. Chem. Soc.*, 2008, **130**, 2902-2903.
11. G. Qi, Y. Wang, L. Estevez, X. Duan, N. Anako, A.-H. A. Park, W. Li, C. W. Jones and E. P. Giannelis, *Energy Environ. Sci.*, 2011, **4**, 444-452.
12. S. A. Didas, A. R. Kulkarni, D. S. Sholl and C. W. Jones, *ChemSusChem*, 2012, **5**, 2058-2064.
13. D. Qian, C. Lei, E.-M. Wang, W.-C. Li and A.-H. Lu, *ChemSusChem*, 2014, **7**, 291-298.
14. R. Lyndon, K. Konstas, B. P. Ladewig, P. D. Southon, P. C. J. Kepert and M. R. Hill, *Angew. Chem. Int. Ed.*, 2013, **52**, 3695-3698.
15. C. Chen, S.-T. Yang, W.-S. Ahn and R. Ryoo, *Chem. Commun.*, 2009, 3627-3629.
16. X. Feng, G. Hu, X. Hu, G. Xie, Y. Xie, J. Lu and M. Luo, *Ind. Eng. Chem. Res.*, 2013, **52**, 4221-4228.
17. S. Choi, J. H. Drese and C. W. Jones, *ChemSusChem*, 2009, **2**, 796-854.
18. Y. Belmabkhout, R. Serna-Guerrero and A. Sayari, *Ind. Eng. Chem. Res.*, 2009, **49**, 359-365.
19. S. Hao, H. Chang, Q. Xiao, Y. Zhong and W. Zhu, *J. Phys. Chem. C*, 2011, **115**, 12873-12882.
20. X. Ma, X. Wang and C. Song, *J. Am. Chem. Soc.*, 2009, **131**, 5777-5783.
21. W.-J. Son, J.-S. Choi and W.-S. Ahn, *Microporous Mesoporous Mater.*, 2008, **113**, 31-40.
22. M. A. Alkhabbaz, R. Khunsupat and C. W. Jones, *Fuel*, 2014, **121**, 79-85.
23. M. R. Mello, D. Phanon, G. Q. Silveira, P. L. Llewellyn and C. M. Ronconi, *Microporous Mesoporous Mater.*, 2011, **143**, 174-179.
24. S. Builes and L. F. Vega, *J. Phys. Chem. C*, 2012, **116**, 3017-3024.
25. P. Bollini, S. A. Didas and C. W. Jones, *J. Mater. Chem.*, 2011, **21**, 15100-15120.
26. H. Vinh-Thang, Q. Huang, A. Ungureanu, M. Eić, D. Trong-On and S. Kaliaguine, *Langmuir*, 2006, **22**, 4777-4786.
27. A. Olea, E. S. Sanz-Pérez, A. Arencibia, R. Sanz and G. Calleja, *Adsorption*, 2013, **19**, 589-600.
28. R. Sanz, G. Calleja, A. Arencibia and E. S. Sanz-Pérez, *Energy Fuels*, 2013, **27**, 7637-7644.
29. G. Calleja, R. Sanz, A. Arencibia and E. S. Sanz-Pérez, *Top. Catal.*, 2011, **54**, 135-145.
30. P. J. E. Harlick and A. Sayari, *Ind. Eng. Chem. Res.*, 2006, **46**, 446-458.
31. A. Heydari-Gorji, Y. Belmabkhout and A. Sayari, *Langmuir*, 2011, **27**, 12411-12416.
32. G. Prieto, A. Martínez, R. Murciano and M. A. Arribas, *Appl. Catal., A*, 2009, **367**, 146-156.
33. Sujandi, E. A. Prasetyanto and S.-E. Park, *Appl. Catal., A*, 2008, **350**, 244-251.
34. J. Sun, H. Zhang, R. Tian, D. Ma, X. Bao, D. S. Su and H. Zou, *Chem. Commun.*, 2006, 1322-1324.
35. H. Gustafsson, E. M. Johansson, A. Barrabino, M. Odén and K. Holmberg, *Colloids Surf., B*, 2012, **100**, 22-30.
36. E. M. Johansson, J. M. Córdoba and M. Odén, *Microporous Mesoporous Mater.* , 2010, **133**, 66-74.
37. P. Linton, H. Wennerstrom and V. Alfredsson, *Phys. Chem. Chem. Phys.*, 2010, **12**, 3852-3858.
38. Sujandi, S.-E. Park, D.-S. Han, S.-C. Han, M.-J. Jin and T. Ohsuna, *Chem. Commun.*, 2006, 4131-4133.
39. A. Heydari-Gorji, Y. Yang and A. Sayari, *Energy Fuels*, 2011, **25**, 4206-4210.
40. S.-Y. Chen, Y.-T. Chen, J.-J. Lee and S. Cheng, *J. Mater. Chem.*, 2011, **21**, 5693-5703.
41. D. Zhao, J. Feng, Q. Huo, N. Melosh, G. H. Fredrickson, B. F. Chmelka and G. D. Stucky, *Science*, 1998, **279**, 548-552.
42. L. Cao, T. Man and M. Kruk, *Chem. Mater.*, 2009, **21**, 1144-1153.
43. A. Goeppert, M. Czaun, R. B. May, G. K. S. Prakash, G. A. Olah and S. R. Narayanan, *J. Am. Chem. Soc.*, 2011, **133**, 20164-20167.
44. Y. G. Ko, S. S. Shin and U. S. Choi, *J. Colloid Interface Sci.*, 2011, **361**, 594-602.
45. A. Sayari, Y. Belmabkhout and E. Da'na, *Langmuir*, 2012, **28**, 4241-4247.
46. M. L. Gray, J. S. Hoffman, D. C. Hreha, D. J. Fauth, S. W. Hedges, K. J. Champagne and H. W. Pennline, *Energy Fuels*, 2009, **23**, 4840-4844.
47. F. Su, C. Lu and H.-S. Chen, *Langmuir*, 2011, **27**, 8090-8098.

48. G. P. Knowles, J. V. Graham, S. W. Delaney and A. L. Chaffee, *Fuel Process.Technol.*, 2005, **86**, 1435-1448.
49. R. V. Siriwardane, M.-S. Shen, E. P. Fisher and J. Losch, *Energy Fuels*, 2005, **19**, 1153-1159.
50. S. Bourrelly, P. L. Llewellyn, C. Serre, F. Millange, T. Loiseau and G. Férey, *J. Am. Chem. Soc.*, 2005, **127**, 13519-13521.
51. D. P. Schrag, *Science*, 2007, **315**, 812-813.
52. K. Masuda, Y. Ito, M. Horiguchi and H. Fujita, *Tetrahedron*, 2005, **61**, 213-229.
53. J. B. Bossa, P. Theule, F. Duvernay, F. Borget and T. Chiavassa, *Astron. Astrophys.*, 2008, **492**, 719-724.
54. J.-B. Bossa, F. Borget, F. Duvernay, P. Theule and T. Chiavassa, *J. Phys. Chem. A*, 2008, **112**, 5113-5120.
55. C. Knoefel, C. Martin, V. Hornebecq and P. L. Llewellyn, *J. Phys. Chem. C*, 2009, **113**, 21726-21734.
56. A. Danon, P. C. Stair and E. Weitz, *J. Phys. Chem. C*, 2011, **115**, 11540-11549.
57. A. Sayari and Y. Belmabkhout, *J. Am. Chem. Soc.*, 2010, **132**, 6312-6314.

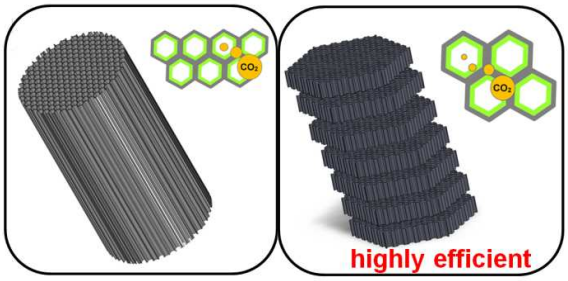

Amine-grafted mesoporous silica materials with short channels and large pore diameter have been prepared and used to adsorb CO_2 efficiently.